40 UNCLASSIFIED Copy 387
RM E54B24

NACA RM E54B24

Classification changed to declassified
effective 1 April 1963 under
NASA CCN 2 by
Carroll.

N63-13865
code 1

RESEARCH MEMORANDUM

PERFORMANCE OF ISENTROPIC NOSE INLETS AT MACH NUMBER OF 5.6

By Harry Bernstein and Rudolph C. Haefeli

Lewis Flight Propulsion Laboratory
Cleveland, Ohio

OTS PRICE

XEROX $ 3.60 pb

MICROFILM $ 1.40 mf

CLASSIFIED DOCUMENT

This material contains information affecting the National Defense of the United States within the meaning of the espionage laws, Title 18, U.S.C., Secs. 793 and 794, the transmission or revelation of which in any manner to an unauthorized person is prohibited by law.

NATIONAL ADVISORY COMMITTEE
FOR AERONAUTICS

WASHINGTON
May 6, 1954

[redacted]

UNCLASSIFIED

NATIONAL ADVISORY COMMITTEE FOR AERONAUTICS

RESEARCH MEMORANDUM

PERFORMANCE OF ISENTROPIC NOSE INLETS AT MACH NUMBER OF 5.6

By Harry Bernstein and Rudolph C. Haefeli

SUMMARY

Performance of inlet configurations with a forebody designed for isentropic external compression was investigated at a nominal Mach number of 5.6 and a Reynolds number based on maximum model diameter of 1.48×10^6. At zero angle of attack all the configurations yielded larger total-pressure recoveries than had previously been obtained with a single-conical-shock inlet. In addition, the internal thrust coefficients were larger for some of the isentropic inlets than for the conical inlet. Performance comparable with that at zero angle of attack was obtained at a 3° angle of attack.

For a configuration having an internal passage with a constant-area section of 2.72 hydraulic diameters, stability was achieved to mass-flow ratios as low as 0.62. With the same configuration, stability was maintained to mass-flow ratios as low as 0.11 by bleeding air through orifices in the forebody near the inlet entrance.

INTRODUCTION

An inlet which efficiently decelerates the air supply is a prime requirement for high-speed flight with an air-breathing engine. Preliminary tests to determine the pressure-recovery and mass-flow ratio characteristics, and hence the efficiencies, of nose inlets at a Mach number near 5.5 are reported in references 1 and 2. These tests yielded performance characteristics of a single-conical-shock inlet and of separation inlets, respectively. Because of reduction in shock losses, diffusers with forebodies having initially small cone angles and followed by a contour designed to produce isentropic external compression should yield larger pressure recoveries than conical inlets. Experimental results have confirmed this expectation for the Mach number range from 2 to 4 (ref. 3).

In addition to the requirement of diffusion efficiency, there exists the necessity of avoiding diffuser instability during reduced mass-flow operation. Several authors have attempted to determine the cause, or triggering action, of diffuser instability. In reference 4 it is proposed that the instability is caused by disturbances propagating upstream in the decelerating flow and becoming trapped in the region of sonic velocity, thus causing a change in the shock structure. The author of reference 5 points out that the vortex sheet originating at the intersection of the inlet shock waves may cause flow oscillations when it enters the inlet. On the basis of these ideas, the analysis of reference 6, and the experimental results of references 7 and 8, the author of reference 9 concludes, and shows experimentally, that the incorporation of a constant-area section downstream of the inlet entrance helps to maintain diffuser stability. During more recent experiments with conical-nose inlets having such constant-area sections, stability was achieved to mass-flow ratios as low as 0.12 at a Mach number of 1.91 (ref. 10).

The tests reported herein were undertaken to determine if an isentropic inlet would yield larger total-pressure recoveries and internal-thrust coefficients than a conical inlet at a Mach number near 5.5. The effects on diffuser stability of a constant-area section in the diffuser passages and mass-flow bleed through orifices in the forebody were also investigated. The tests were conducted at the NACA Lewis laboratory.

SYMBOLS

The following symbols are used in this report:

A area

M Mach number

m mass-flow rate

P total pressure

γ ratio of specific heats, 1.4 for air

η_{KE} kinetic-energy efficiency,

$$\frac{\text{kinetic energy of air expanded isentropically from diffuser exit to free-stream static pressure}}{\text{free stream kinetic energy}}$$

[redacted]

Subscripts:

0 free-stream tube having a diameter equal to the cowl diameter at the cowl leading edge

1 combustion-chamber conditions

APPARATUS

Wind tunnel. - The tests were conducted in the Lewis 6- by 6-inch continuous-flow hypersonic tunnel at a nominal Mach number of 5.6. The small increase in Mach number above the values in references 1 and 2 was believed caused by changes in the boundary-layer growth and other factors associated with the increased pressure level at which the tunnel was operated during the present tests. The test-section total pressure was maintained between 322 and 353 pounds per square inch absolute, with a variation of less than ±2.0 pounds per square inch during any one run. The stagnation temperature was 267° ±6° F. The test-section Reynolds number, based on an average total pressure of 335 pounds per square inch absolute and on maximum model diameter, was 1.48×10^6.

Some indications of partial condensation of the air components were obtained through use of the light-scattering technique described in reference 11. The appearance of condensation (not observed at the test conditions of refs. 1 and 2) was attributed to operation at large total pressures, such that the saturation temperature of the air components was greater than the test-section static temperature (ref. 11).

The analysis of reference 12 indicates that the free-stream Mach number for the partially condensed flow can be determined with an accuracy sufficient for the present tests if pitot and static pressures are measured and the Mach number is computed from the Rayleigh equation. The pressure recovery and mass-flow ratio of the inlet are based on the free-stream total pressure computed for the Rayleigh Mach number and are believed, therefore, to be negligibly affected by the condensation.

The pitot- and static-pressure probes described in reference 13 were used in the calibration of the tunnel. The pressures were measured with mercury and butyl phthalate manometers, respectively.

Schlieren photographs of the flow about the model were obtained with an exposure time of approximately 2 microseconds.

Model. - The basic inlet configuration is shown in figures 1 and 2. The isentropic forebody, designed for a Mach number of 5.5, had an initial cone half-angle of 9.9° and was designed to compress the flow to Mach number 2.4 at the inlet entrance. No correction was made for boundary-layer growth on the external-compression surface; the results herein should therefore not be construed to be those of an optimum design. The external cowl contour had an initial lip angle of 39°, which is less than the shock detachment angle for a Mach number of 5.6 (42.0°). For this design, the theoretical total-pressure recovery is 0.48, based on losses through the forebody tip shock and the diffuser terminal shock (at Mach number of 2.4) and on an estimated 5-percent loss through the subsonic diffuser.

During the course of the investigation, it was observed that factors such as boundary-layer growth, boundary-layer separation, and machining inaccuracies acted to change the flow configuration from that assumed in the design of the inlet. In an effort to offset these effects and capture a complete free-stream tube, small changes in the geometry of the inlet were made and the effects of these investigated. Two cowls and two forebodies were employed which differed only in their distribution of internal passage area (fig. 3(a)). Additional geometry changes were effected by varying the position of the forebody relative to the cowl. The forebody coordinates are presented in table I, and the cowl coordinates are given in table II. Translation of the forebody from the reference position (fig. 2) was accomplished by inserting or removing shims between the forebody and the centerbody. The effect of this translation upon inlet geometry was that the inlet entrance area decreased as the forebody was moved forward (fig. 3(b)). Forebody translation had no effect on the internal areas at stations more than 0.5 inch from the inlet entrance. (For the remainder of the report, forward translations of the forebody will be indicated by a plus (+) sign and backward translations by a minus (-) sign.) Only two of the configurations tested had internal contraction:

(1) Cowl A; forebody A; zero translation; internal-contraction ratio, 1.243.

(2) Cowl B; forebody A; translation of -0.01 inch; internal-contraction ratio, 1.032.

Inlet characteristics were also obtained with roughness (number 80 silicon carbide grit) on the forebody tip to induce transition of the boundary layer.

[redacted]

For several tests, two rows of 36 orifices with 1/8-inch diameters were drilled in forebody B immediately downstream of the inlet entrance (fig. 4) in order to bleed air from the surface of the forebody and thus delay separation of the boundary layer. This air was exhausted through the center of the model to the wind tunnel.

The model instrumentation, described in reference 2, is visible in figure 1(b). The pressures were measured with a differential mercury manometer.

REDUCTION OF DATA

The results of a Mach number survey at an axial station $33\frac{3}{4}$ inches downstream of the tunnel throat are presented in figure 5. The model was located with the tip of its forebody at a station $33\frac{1}{8}$ inches from the tunnel throat. The Mach numbers, determined by use of the Rayleigh equation from pitot- and static-pressure measurements, were reproducible within 3 percent. Inasmuch as the variations from a Mach number of 5.6, indicated in figure 5, are generally within the reproducibility, a nominal Mach number of 5.6 was chosen for computations of inlet performance.

The test-section pitot pressure was measured at locations approximately 3/4-inch ahead of the cowl leading edge after each model test. The free-stream total pressure was computed from these measurements and from the normal-shock relations for a Mach number of 5.6.

The method of computation of diffuser pressure recovery and mass-flow ratio was the same as that described in reference 2. The pressure recoveries and mass-flow ratios reported for stable operation are estimated to be accurate to within 1 percent of their values. The data for unstable operation represent time-average values; the pressures appeared constant on the manometers because of inertia of the manometer system. Therefore, no estimate of accuracy has been made for these data, which should be used only as a qualitative indication of performance.

DISCUSSION OF RESULTS

Flow about Forebody

An enlarged schlieren photograph of the flow over the forebody (diffuser cowl removed) is presented in figure 6. There is

no evidence of boundary-layer separation along the external-compression surface. The curvature of the tip shock at its downstream end indicates that the compression waves generated by the forebody did not meet at a point. This is attributed to design and machining inaccuracies and to the boundary layer, all of which change the forebody contour from an isentropic compression surface.

3103

Inlet Performance

The variations of total-pressure recovery $\frac{P_1}{P_0}$ with mass-flow ratio $\frac{m_1}{m_0}$ at zero and 3° angles of attack are shown in figures 7 to 13 for the various configurations tested. Figures 14 to 19 present typical schlieren photographs of the flow configurations.

A summary chart of the performances is given in table III. The values of the kinetic-energy efficiency were computed for the operating Mach number of 5.6 from the equation

$$\eta_{KE} = 1 - \frac{\left(\frac{P_0}{P_1}\right)^{\frac{\gamma - 1}{\gamma}} - 1}{\frac{\gamma - 1}{2} M_0^2}$$

Also included in the table for comparison are the performance figures for a single-conical-shock inlet tested during the present investigation. The conical inlet, which was the same model discussed in reference 1, was operated with the cone retracted 0.01 inch from its original design location and with roughness on the cone tip. This was the optimum configuration, as indicated in reference 1. Its peak recovery is 2.9 percent lower than that given in reference 1. This decrease was believed caused by the higher Mach number at which the present tests were conducted.

Effect of roughness. - From the summary chart it is seen that at zero angle of attack the use of roughness on the forebody tip caused an increase in the mass-flow ratio at peak recovery, although there was a decrease in the maximum pressure recovery. At a 3° angle of attack, the presence of roughness had essentially no effect on the mass-flow ratio at peak recovery, but the total-pressure recovery increased slightly.

With no roughness, boundary-layer separation within the inlet was indicated by the decreasing mass-flow ratio in the stable operating range as maximum recovery was approached (figs. 7 and 9(a)). The use of roughness was a sufficient means for preventing this separation (fig. 7) except for operation close to maximum recovery (fig. 9(b)).

During unstable operation, when no roughness was used, separation of the boundary layer at the forebody tip occurred as soon as the outlet area was decreased beyond its value at maximum recovery (figs. 15(a) and 17(a)). The application of roughness to the forebody tip resulted in intermittent separation and reattachment of the forebody boundary layer when the outlet area was only slightly below its value at maximum recovery. Hence, operation at intermediate values of pressure recovery and mass-flow ratio was permitted, in contradistinction to operation without roughness (e.g., cf. fig. 10(a) with fig. 10(b)). For unstable operation with roughness, the terminal shock oscillated over the forebody ahead of the inlet entrance (figs. 15(b) and 17(b)), except for the intermittent periods during which separation occurred at the forebody tip.

Effect of cowl and forebody contour. - The effects of cowl and forebody changes are considered for a forebody translation of zero. With no roughness, at both zero and 3° angles of attack, a change from cowl A to cowl B, while still using forebody A, resulted in reduction of both the peak pressure recovery and the mass-flow ratio. The reduction in mass flow was believed to be caused by a forward movement of the boundary-layer separation point within the inlet, resulting in a smaller effective throat area. Figure 3 shows that between axial stations 0.12 and 0.66 the internal area decreases less for cowl B than for cowl A. Hence, the pressure gradient in the region (subsonic flow) was less favorable for cowl B, which may account for the forward movement of the separation point. The reduction in total-pressure recovery was caused by the increased flow spillage which resulted in a forward movement (into a higher Mach number region) of the terminal shock.

With roughness, at zero angle of attack, the change to cowl B resulted in an increase in the total-pressure recovery and a decrease in the mass-flow ratio at peak recovery. A comparison of figures 7 and 9(b) shows that these changes are caused by the increased stability range of the cowl B and forebody A combination. The increase in internal passage areas also resulted in a larger maximum mass-flow ratio.

The cowl B and forebody B combination, at zero angle of attack (fig. 11), showed stability over a considerable mass-flow ratio range (to ratios as small as 0.62). This combination had an internal passage which incorporated a constant-area section of 2.72 hydraulic diameters, located as shown in figure 3. The results for a forebody translation of -0.010 inch (fig. 11(b)) are unusual in that a dip in the recovery occurred as the mass-flow ratio was decreased from 0.87 to 0.62. The flow was unstable; that is, the terminal shock oscillated over the forebody ahead of the inlet entrance when the slope of the pressure-recovery mass-flow ratio curve was positive, as predicted in reference 6. In general, this combination yielded lower maximum total-pressure recoveries and mass-flow ratios than the two previous combinations. The mass-flow ratio at maximum recovery with no roughness was larger, however, than both of the other cowl and forebody combinations at zero angle of attack.

Effect of bleed through forebody. - The performance curves of figure 13 show the large ranges of mass-flow ratio in which stable operation occurred after orifices were drilled in forebody B for bleeding air out of the entrance annulus (to ratios as small as 0.11). With no bleed through these orifices, the performance for a zero forebody translation was essentially the same as was obtained before the orifices were drilled (fig. 11(b)). Hence, the increased range of stability can be attributed solely to the bleeding rather than to surface roughness caused by the presence of the orifices. There was, however, a decrease in the maximum mass-flow ratio because some of the flow was bypassed through the orifices. The inlet, of course, could be designed to bleed only when stable flow at low mass-flow ratios is required.

In certain intermediate ranges of mass-flow ratio, schlieren observations indicated oscillations of the diffuser terminal shock. Data taken in this range of operation are indicated by tailed symbols. The reasons for this instability have not been determined.

Figure 19 is a schlieren photograph of the inlet with bleed through the forebody operating at a mass-flow ratio of 0.18. Inasmuch as the terminal shock is at about the same location relative to the cowl as in previous photographs pertaining to operation without bleed at substantially larger mass-flow ratios (fig. 18(a), e.g.), apparently much of the flow is being discharged through the bleed system. In fact, the forebody orifices provide a bypass of varying mass-flow capacity because the entrance static pressure (at orifice) increases with a decrease in mass-flow ratio (forward movement of the terminal shock) as shown in figure 20. The terminal shock, therefore, need not move as far forward of the inlet entrance as it would if the same amount of mass flow were spilled entirely

[redacted]

ahead of the inlet. The present bypass arrangement thus maintains the additive drag of the inlet near a minimum throughout a large range of mass flows without requiring changes in bypass area and, at the same time, provides diffuser stability.

Effect of forebody translation. - The effects of forebody translation were essentially the same for each of the configurations for which translation was investigated. The effects will therefore be discussed for the cowl B and forebody A combination operating at zero angle of attack.

With no roughness, increases in the forebody translation up to +0.020 inch resulted in increases in the peak total-pressure recovery, while no change occurred in the mass-flow ratio at peak recovery or in the maximum mass-flow ratio. For a +0.020-inch translation (fig. 9(a)), the mass-flow ratios were higher over most of the stable range.

With roughness on the forebody tip, the maximum mass-flow ratio was the same for both the zero and +0.010-inch translations. Failure of the mass-flow ratio to change with the forebody translation and the concurrent entrance area change indicates the presence of an effective minimum-area section within the diffuser caused by the boundary layer. A +0.020-inch translation resulted in a decrease in the maximum mass-flow ratio because of the reduction in the effective minimum passage area (now located at the inlet entrance). The decrease in maximum mass-flow ratio obtained with a -0.010-inch translation was caused by the relocation of the bow wave in a region of higher Mach number. The resulting increased total-pressure losses require, for the same minimum passage area, a decrease in the mass flow. Peak performance was essentially independent of forebody translation, except for a +0.020-inch translation for which the maximum recovery was increased but the mass-flow ratio reduced.

Effect of angle of attack. - With no roughness, the change from zero to a 3° angle of attack generally caused a decrease in the peak pressure recovery. The mass-flow ratio, however, was increased throughout the stable range (for a given recovery) for almost all the configurations tested.

With roughness, operation at a 3° angle of attack generally had little effect on the maximum total-pressure recovery but produced a decrease in the mass-flow ratio at peak recovery. For operation with cowl B and forebody B, stability was achieved, as for zero-angle-of-attack operation, over a range of mass-flow ratios, except for +0.02-inch forebody translation (fig. 12(b)). For a -0.01-inch translation, the stability was obtained only at a

negative angle of attack. This effect may be caused by eccentricity of the cowl and forebody or by tunnel flow irregularities. For the cowl B and forebody B configuration with bleed (fig. 13(b)), the recovery was maintained to mass-flow ratios as low as 0.14, although in an intermediate range of mass-flow ratios the terminal shock was unsteady.

Performance Comparisons

A comparison of the performances of the conical and isentropic nose inlets shows that, at both zero and 3° angles of attack, total-pressure recoveries, and hence kinetic-energy efficiencies, significantly greater than those of the conical-nose inlet were obtained with the models of the present investigation. The mass-flow ratios of the isentropic configurations were, in all cases, less than that of the conical inlet.

Some typical internal thrust coefficients (based upon A_0) for zero-angle-of-attack operation have been calculated for engines with the conical and isentropic inlets. The internal thrust force is that caused by the change of momentum of the air flowing through the engine. In these calculations, the following factors were assumed:

(1) Flight at 43,000 feet (This would make the flight and test Reynolds numbers equal.)

(2) Completely expanded exit

(3) Heating value of fuel of 18,000 Btu per pound

(4) Fuel-air ratio of 0.03; combustion efficiency of 0.9

(5) Mach number at entrance to combustion chamber of 0.15

The results of the internal-thrust-coefficient computations are given in table IV.

As shown in this table, internal thrust coefficients somewhat larger than those of the conical inlet are obtainable with several of the isentropic configurations. For some of the configurations, larger values of internal thrust could be obtained for operation with less than maximum recovery but with a larger mass-flow ratio. This results because the kinetic-energy efficiency does not change much with pressure recovery in the present range of recovery and Mach number. No attempt was made to find the optimum operating point for a configuration. Thrust

3103

coefficients for 3° angle-of-attack operation have approximately the same magnitude as those for zero-angle-of-attack operation, since there was, in general, little change in pressure recovery and mass-flow ratio with angle of attack.

Because the isentropic inlets operate at mass-flow ratios less than 1, the penalty of additive drag associated with the flow spillage must be incurred. This deficiency in the performance of isentropic inlets might be avoided by further developmental changes in the diffuser design. Any modifications serving to reduce the additive drag would also serve to increase the internal thrust because of the increase in captured mass flow.

It is important to note that the higher combustion-chamber pressures obtained with the isentropic inlets might be a necessity for efficient combustion during high-altitude flight. Also, the higher recoveries result in smaller required combustion-chamber areas when a comparison is made on a basis of equal mass-flow rates m_1 and combustion-chamber Mach numbers M_1. As a result, the high-recovery inlet has the advantage of having more space (between the combustion chamber and external contour) available for auxiliary equipment.

The values of internal thrust calculated for the inlets with bleed are small because of the small maximum mass-flow ratios. It was assumed that no momentum was recovered from the bypassed air. Except when off-design performance with small exit mass flow is required, the inlet could be operated without bleed to maintain large values of thrust during flight at design conditions.

SUMMARY OF RESULTS

Performance of inlets with a forebody designed for isentropic external compression was investigated in the Lewis 6- by 6-inch hypersonic tunnel at a nominal Mach number of 5.6 and a Reynolds number based on maximum model diameter of 1.48×10^6. The configurations tested involved two cowls and two forebodies which differed only in their distribution of internal passage area. The effects of roughness on the forebody tip to induce transition of the boundary layer, of varying the position of the forebody, and of bleeding air from the surface of the centerbody were also investigated. Results of these test are as follows:

1. At both zero and 3° angles of attack, all the isentropic configurations yielded larger total-pressure recoveries than had previously been obtained with a single-conical-shock

inlet. None of the configurations, however, was able to capture a full free-stream tube. The internal thrust coefficients were larger for some of the isentropic inlets than for the single-conical-shock inlet.

2. For the configurations having internal passages with a constant-area section of 2.72 hydraulic diameters, stable flow was obtained over a large range of mass-flow ratios. By bleeding air from the surface of the forebody immediately downstream of the inlet entrance, the range of stable flow was extended to mass-flow ratios as low as 0.11. For configurations without a constant-area section and without bleed, the flow was unstable at mass-flow ratios less than that at peak recovery.

3. The use of roughness on the forebody tip was sufficient measure to prevent boundary-layer separation within the inlet during stable operation, except in the vicinity of maximum recovery. In addition, with roughness the inlet could operate (unstably) at intermediate values of the total-pressure recovery and mass-flow ratio in contradistinction to operation without roughness. This effect was most pronounced at angle of attack.

Lewis Flight Propulsion Laboratory
National Advisory Committee for Aeronautics
Cleveland, Ohio, March 8, 1954

REFERENCES

1. Bernstein, Harry, and Haefeli, Rudolph C.: Investigation of Pressure Recovery of a Single-Conical-Shock Nose Inlet at Mach Number 5.4. NACA RM E53A12, 1953.

2. Haefeli, Rudolph C., and Bernstein, Harry: Performance of Separation Nose Inlets at Mach Number 5.5. NACA RM E53I23, 1953.

3. Cortright, Edgar M., Jr., and Connors, James F.: Survey of Some Preliminary Investigations of Supersonic Diffusers at High Mach Numbers. NACA RM E52E20, 1952.

4. Kantrowitz, Arthur: The Formation and Stability of Normal Shock Waves in Channel Flows. NACA TN 1225, 1947.

5. Ferri, Antonio, and Nucci, Louis M.: The Origin of Aerodynamic Instability of supersonic Inlets at Subcritical Conditions. NACA RM L50K30, 1951.

6. Sterbentz, William H., and Evvard, John C.: Criterions for Prediction and Control of Ram-Jet Flow Pulsations. NACA RM E51C27, 1951.

7. Wyatt, DeMarquis D., and Hunczak, Henry R.: An Investigation of Convergent-Divergent Diffusers at Mach Number 1.85. NACA RM E50K07, 1951. (Supersedes NACA RM E6K21.)

8. Dailey, C. L.: Diffuser Instability in Subcritical Operation. Univ. Southern Calif., Sept. 26, 1950.

9. Nettles, J. C.: The Effect of Initial Rate of Subsonic Diffusion on the Stable Subcritical Mass-Flow Range of a Conical Shock Diffuser. NACA RM E53E26, 1953.

10. Beheim, Milton, A: A Preliminary Investigation at Mach Number 1.91 of a Diffuser Employing a Pivoted Cone to Improve Operation at Angle of Attack. NACA RM E53I30, 1953.

11. Hansen, C. Frederick, and Nothwang, George J.: Condensation of Air in Supersonic Wind Tunnels and its Effects on Flow about Models. NACA TN 2690, 1952.

12. Nagamatsu, H. T., and Grey, J.: The Effects of Air Condensation on Properties of Flow and Their Measurement in Hypersonic Wind Tunnels. Mem. No. 8, Guggenheim Aero. Lab., C.I.T., June 15, 1952. (Sponsored by Army Ord. and Air Force, Contract DA-04-495-Ord-19.)

13. Haefeli, Rudolph C.: Use of Fences to Increase Uniformity of Boundary Layer on Side Walls of Supersonic Wind Tunnels. NACA RM E52E19, 1952.

3103

TABLE I. - FOREBODY COORDINATES FOR ISENTROPIC INLET

(a) Forebody A

Station distance from forebody tip, in.	Forebody radius, in.	Station distance from forebody tip, in.	Forebody radius, in.
0	0	2.700	0.6233
.100	.0175	2.800	.6977
.200	.0351	2.825	.7160
.300	.0525	2.850	.7299
.400	.0700	2.900	.753
.500	.0875	3.000	.783
.600	.1049	3.100	.803
.700	.1233	3.200	.815
.800	.1400	3.300	.823
.900	.1574	3.400	.828
1.000	.1750	3.500	.830
1.100	.1924	3.600	.828
1.200	.2100	3.700	.825
1.300	.2274	3.800	.818
1.400	.2449	3.900	.810
1.500	.2623	4.000	.801
1.600	.2798	4.100	.792
1.700	.3010	4.200	.783
1.800	.3234	4.300	.775
1.900	.3450	4.400	.767
2.000	.3695	4.500	.758
2.100	.3951	4.600	.750
2.200	.4239	4.700	.741
2.300	.4554	4.800	.732
2.400	.4896	4.900	.724
2.500	.5273	5.000	.715
2.600	.5701	5.100	.707

[redacted]

TABLE I. - Concluded. FOREBODY COORDINATES FOR ISENTROPIC INLET

(b) Forebody B

[Coordinates of other stations are same as for forebody A.]

Station distance from forebody tip, in.	Forebody radius, in.
3.0	0.783
3.1	.798
3.2	.806
3.3	.811
3.4	.814
3.5	.815
3.6	.815
3.7	.814
3.8	.811
3.9	.806
4.0	.800
4.1	.792

TABLE II. - COWL COORDINATES FOR ISENTROPIC INLET

(a) Cowl A

Station distance from cowl lip, in.	Cowl inside radius, in.	Cowl outside radius, in.
0	0.787	0.787
.035	.807	.820
.085	.830	.860
.185	.857	.917
.285	.869	.945
.385	.874	.960
.485	.875	.968
.585	.875	.973
.685	.875	.975
.885	.875	.975
1.085	.875	.975
1.185	.875	.975
1.385	.875	.975
1.485	.875	.975
1.585	.875	.975
1.685	.875	.975
1.785	.875	.975
1.885	.875	.975

(b) Cowl B

[Outside radii same as for cowl A.]

Station distance from cowl lip, in.	Cowl inside radius, in.
0	0.787
.035	.807
.085	.830
.185	.857
.285	.873
.385	.882
.485	.886
.585	.887
.685	.888
.885	.888
1.085	.888
1.185	.888
1.385	.827
1.485	.885
1.585	.881
1.685	.878
1.785	.876
1.885	.875

TABLE III. - SUMMARY OF PERFORMANCE OF INLETS

	Forebody translation, in.	Roughness					No roughness		
		Cowl A; forebody A	Cowl B; forebody A	Cowl B; forebody B	Cowl B; forebody B with bleed	Single-conical-shock inlet	Cowl A; forebody A	Cowl B; forebody A	Cowl B; forebody A
Zero angle of attack									
Maximum total-pressure recovery, percent	-0.01 0 +0.01 +.02	17.5	17.7 18.4 18.0 19.9	15.4 15.6 17.4 19.5	17.6 17.2 20.6	10.8	19.5	18.7 19.7 20.8	15.9
Maximum kinetic energy efficiency, percent	-0.01 0 +.01 +.02	89.7	89.8 90.1 89.9 90.7	88.7 88.8 89.6 90.5	89.8 89.6 90.9	85.8	90.5	90.2 90.6 91.0	89.0
Mass-flow ratio at maximum recovery	-0.01 0 +.01 +.02	0.93	0.88 .88 .89 .77	0.87 .74 .84 .63	0.16 .20 .10	1.00	0.84	0.76 .76 .75	0.87
Maximum mass-flow ratio	-0.01 0 +.01 +.02	0.93	0.91 .97 .97 .85	0.88 .91 .91 .87	0.83 .82 .81	1.00	0.93	0.87 .87 .87	0.90
Figure		7	9(b)	11(b)	13(a)	-----	7	9(a)	11(a)
Angle of attack, 3°									
Maximum total-pressure recovery, percent	-0.01 0 +.01 +.02		18.7 18.7 18.7 19.9	15.9 17.7 17.9 17.6	17.7	11.5	17.3	16.9 18.6 19.1	16.4
Maximum kinetic energy efficiency, percent	-0.01 0 +.01 +.02		90.2 90.2 90.7	89.0 89.8 89.9 89.8	89.8	86.4	89.6	89.5 90.2 90.4	89.3
Mass-flow ratio at maximum recovery	-0.01 0 +.01 +.02		0.75 .78 .80	0.84 .65 .66 .80	0.14	0.96	0.94	0.74 .84 .85	0.89
Maximum mass-flow ratio	-0.01 0 +.01 +.02		0.84 .88 .87	0.87 0.88 .88 .84	0.80	0.98	0.94	0.85 .90 .87	0.92
Figure			10(b)	12(b)	13(b)	-----	8	10(a)	12(a)

TABLE IV. - INTERNAL THRUST COEFFICIENTS

Fore-body	Cowl	Forebody translation, in.	Total-pressure recovery	Mass-flow ratio	Internal thrust coefficient
No roughness					
A	A	0	0.195	0.84	0.46
A	B	0	0.187	0.76	0.41
		+0.01	0.197	0.76	0.41
		+0.02	0.208	0.75	0.41
			0.204	0.83	0.46
			0.158	0.87	0.44
B	B	0	0.153	0.90	0.46
Roughness					
A	A	0	0.175	0.93	0.49
A	B	-0.01	0.177	0.88	0.47
		0	0.184	0.88	0.47
		+0.01	0.180	0.89	0.47
			0.173	0.94	0.50
			0.142	0.97	0.48
		+0.02	0.199	0.77	0.42
B	B	-0.01	0.154	0.87	0.44
		+0.01	0.174	0.84	0.44
			0.162	0.88	0.45
B with bleed	B	0	0.142	0.78	0.38
		+0.01	0.116	0.74	0.34
		+0.02	0.128	0.78	0.37
Single-conical-shock inlet			0.108	1.00	0.46

[redacted]

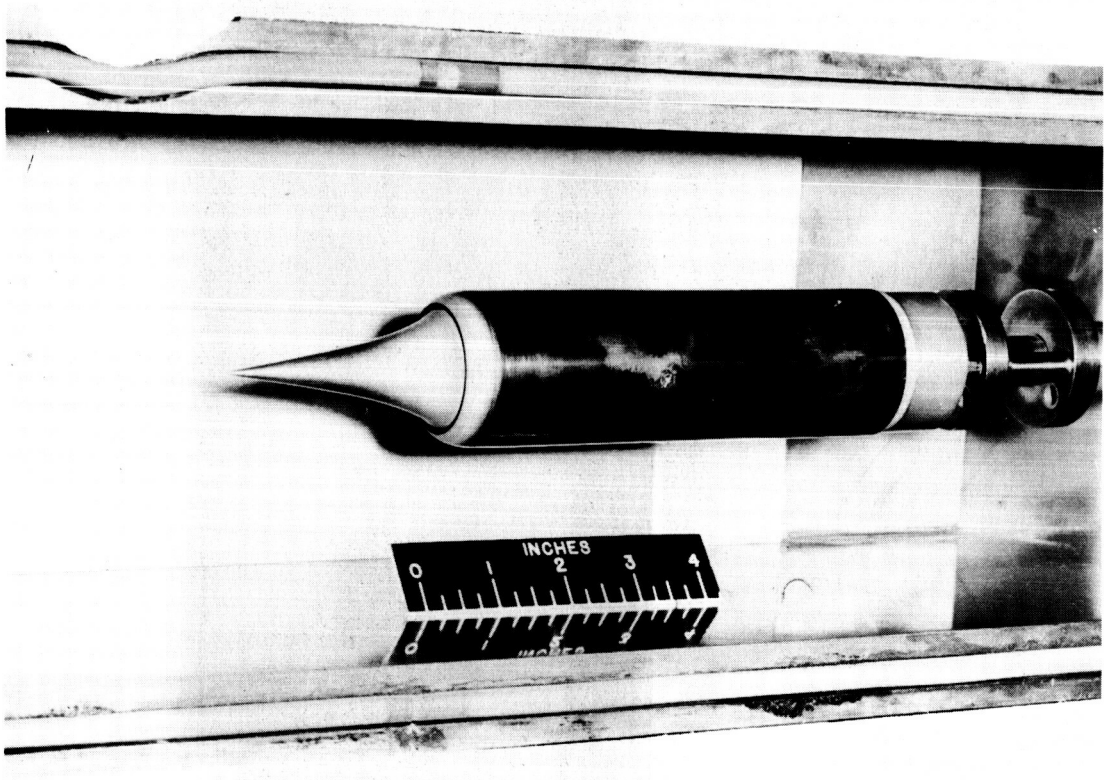

C-33395

(a) Model assembled.

Figure 1. - Isentropic inlet mounted in Lewis 6- by 6-inch hypersonic tunnel.

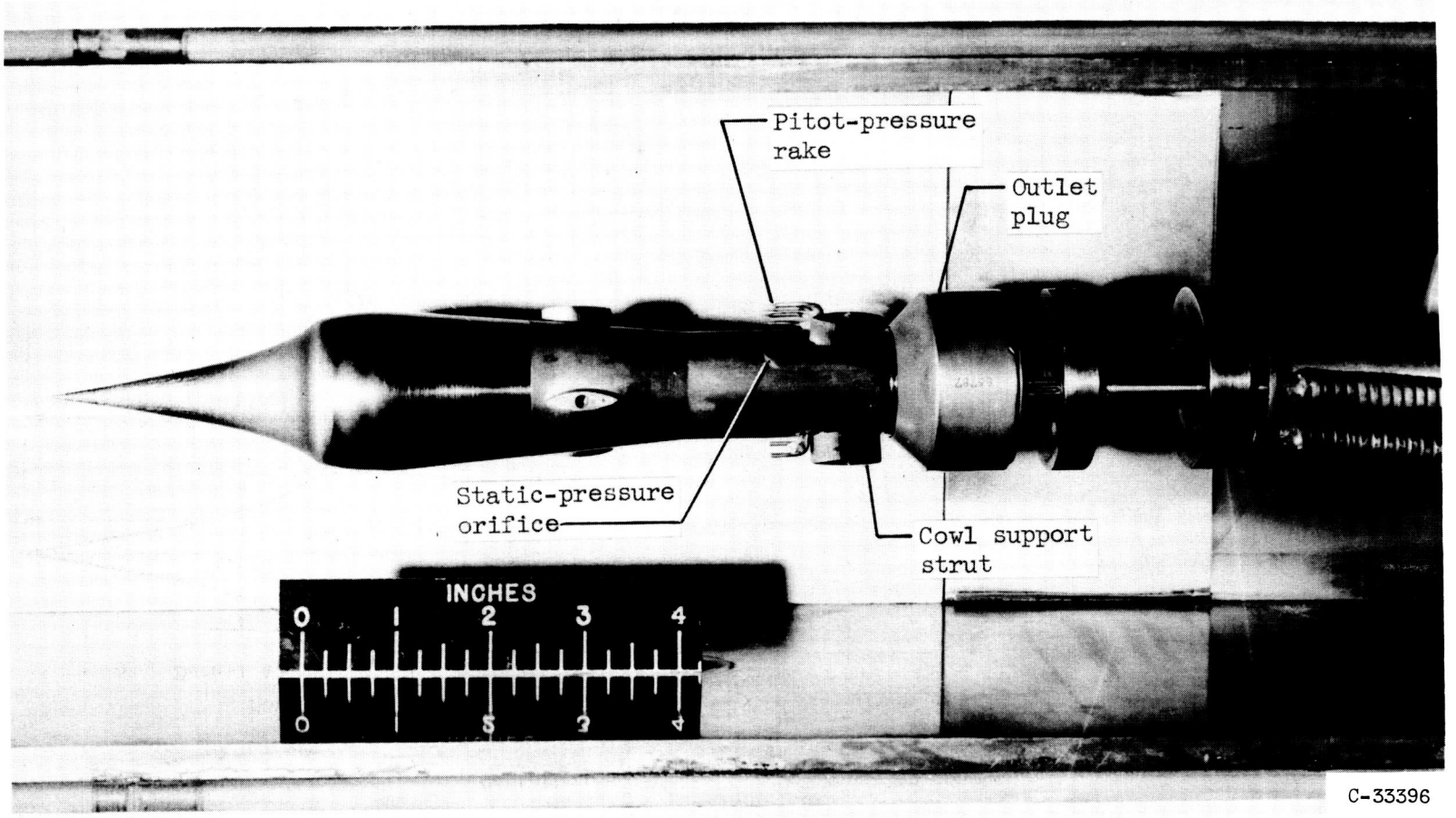

(b) Cowl removed to show instrumentation.

Figure 1. - Concluded. Isentropic inlet mounted in Lewis 6- by 6-inch hypersonic tunnel.

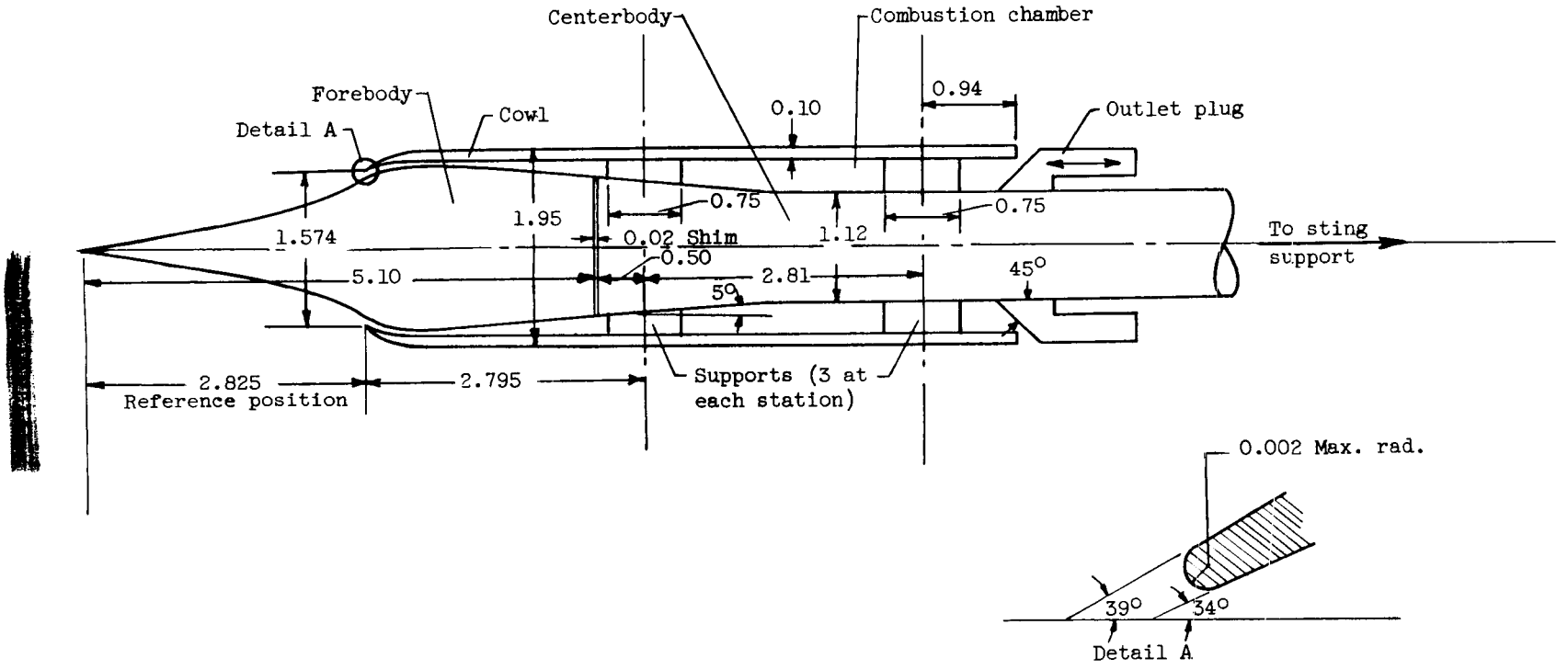

Figure 2. - Isentropic inlet. (All dimensions in inches.)

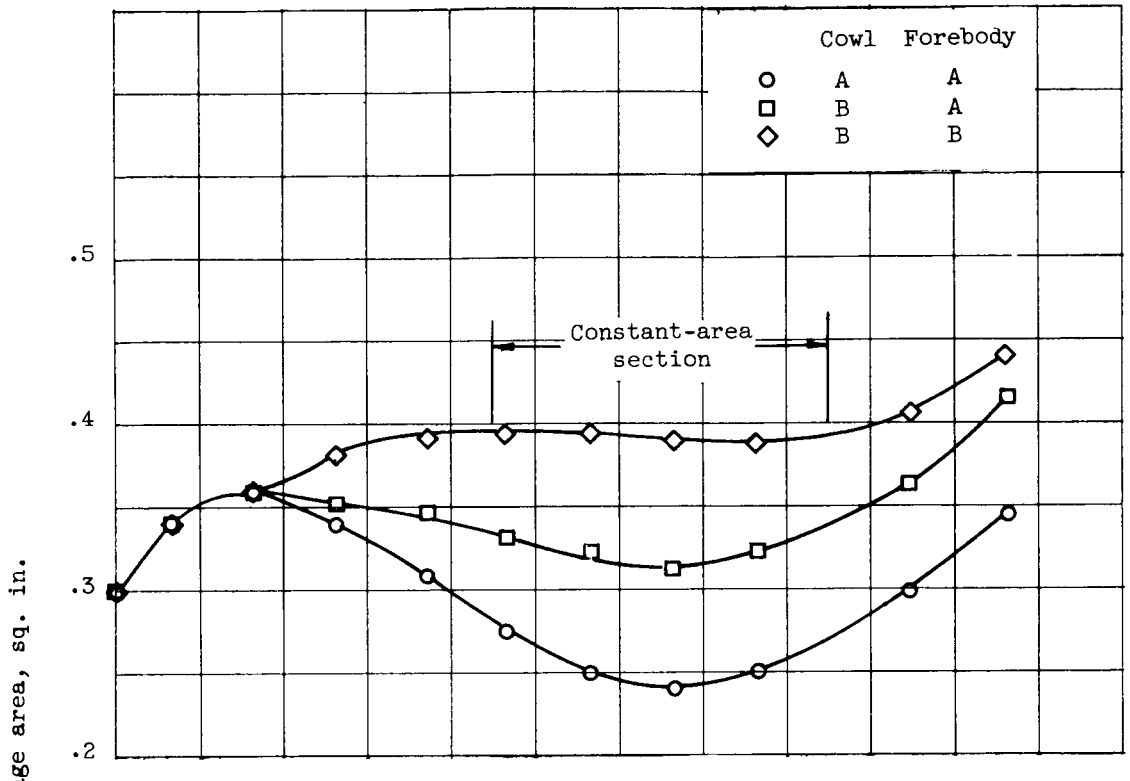

(a) Zero forebody translation; effects of cowl and forebody changes.

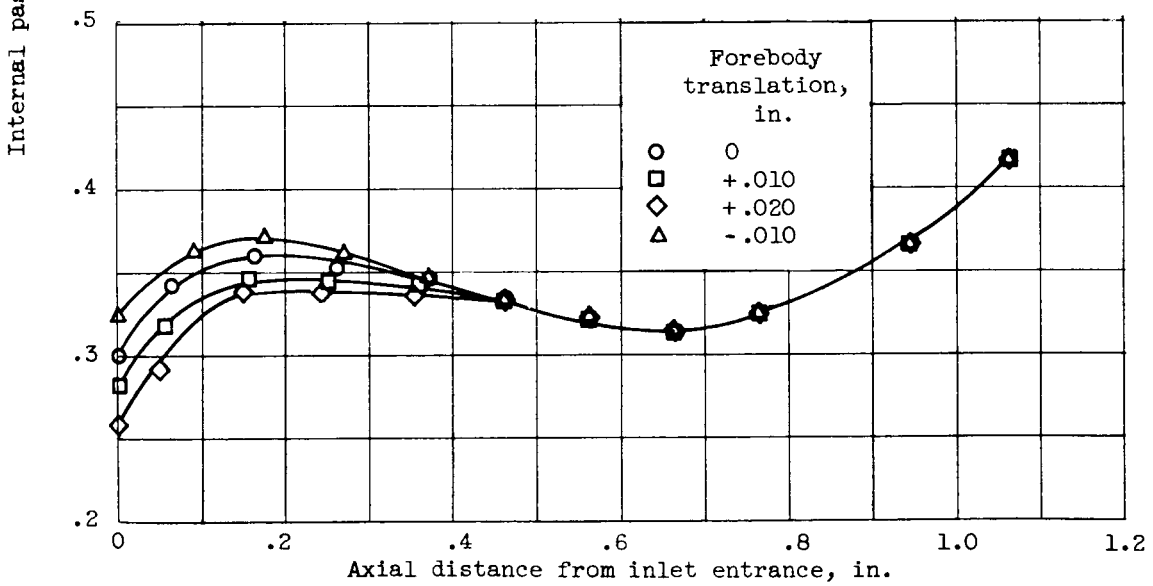

Internal passage area, sq. in.

(b) Cowl B; forebody A; effects of forebody translation.

Figure 3. - Internal-passage-area distribution.

[redacted]

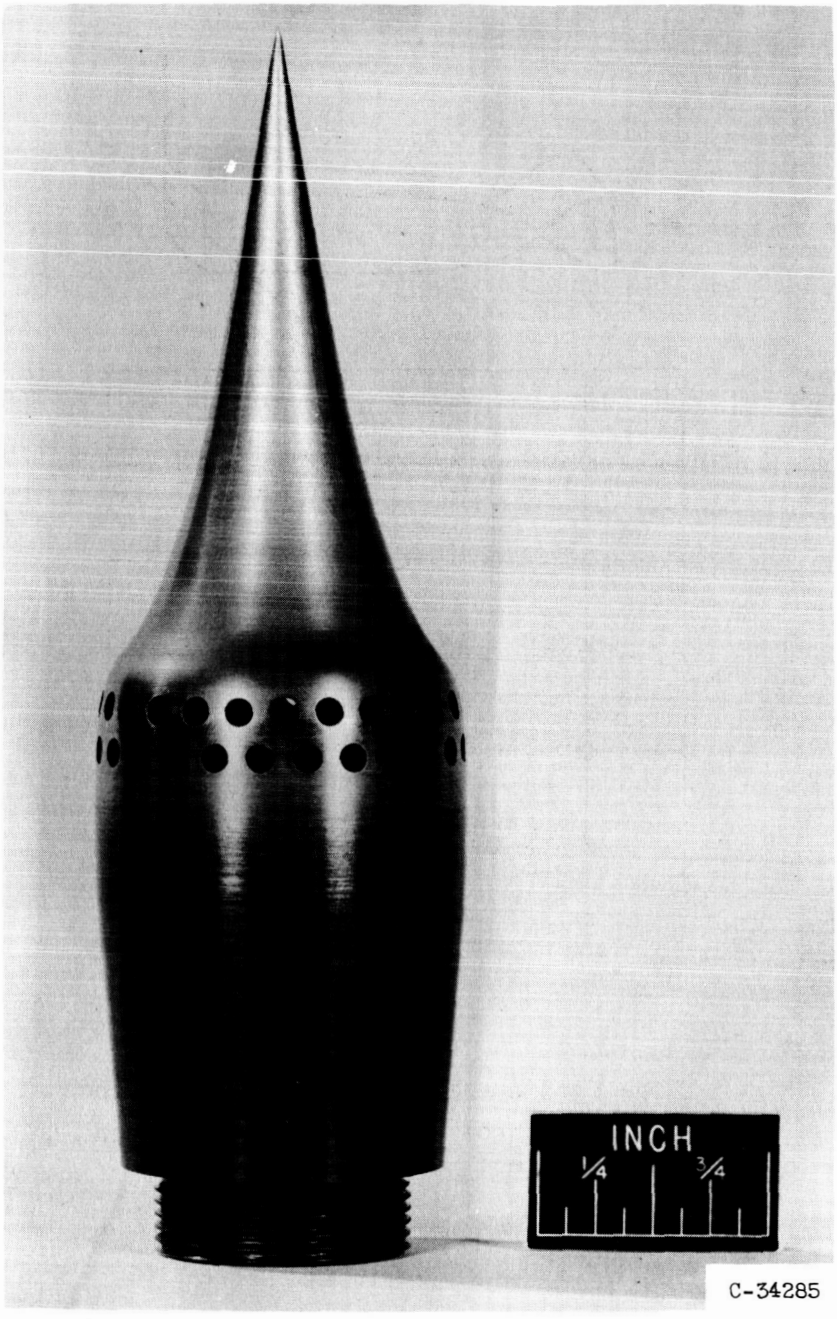

Figure 4. - Forebody B with orifices for bleeding air from surface.

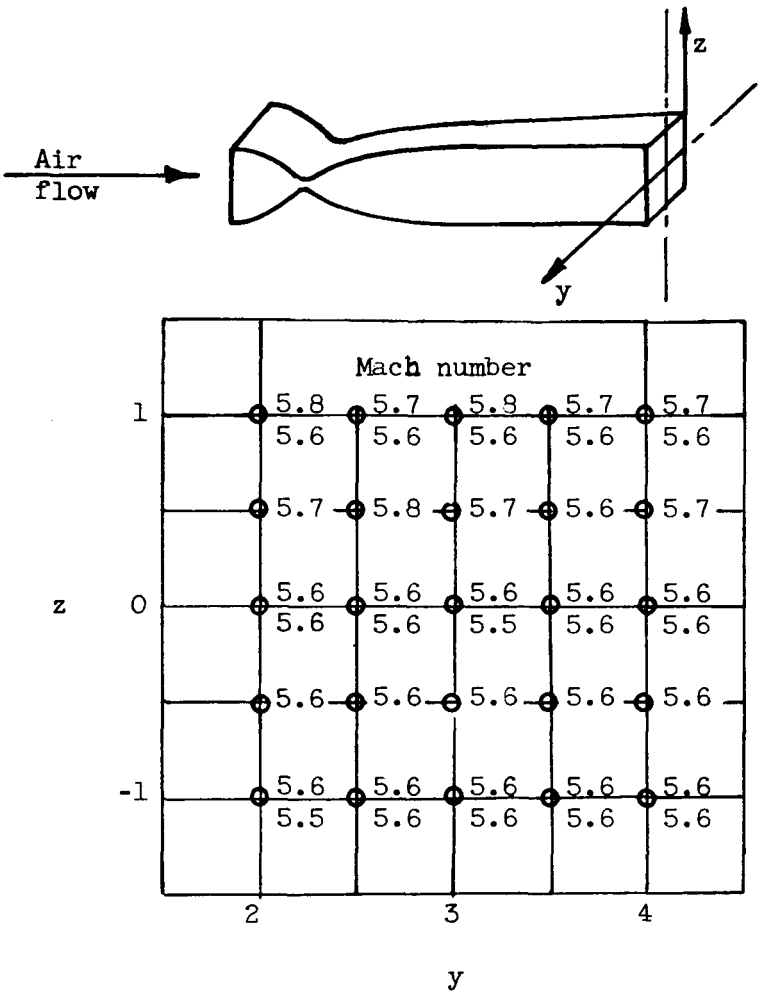

Figure 5. - Mach number calibration $33\frac{3}{4}$ inches downstream of throat of Lewis 6- by 6-inch hypersonic tunnel.

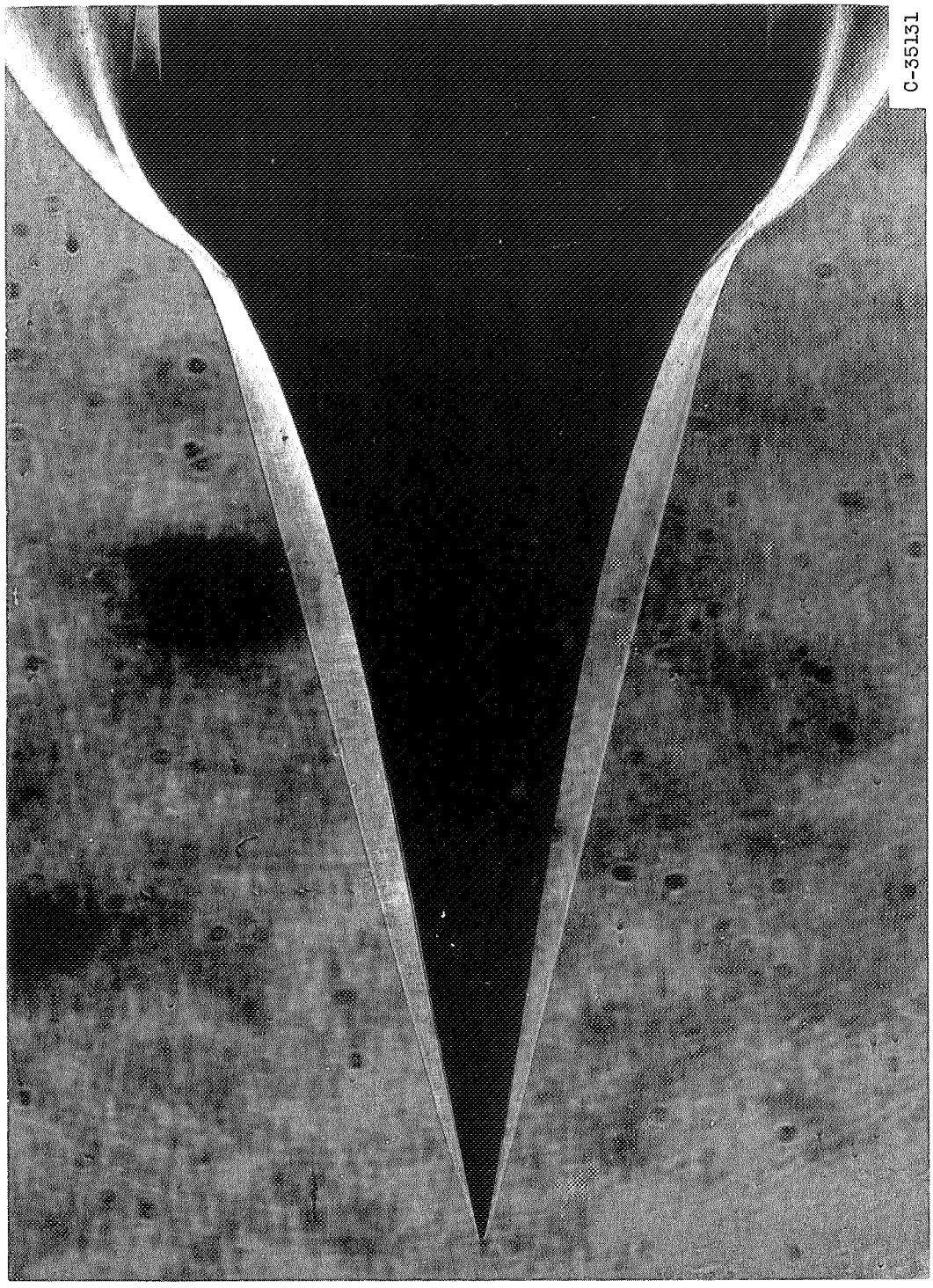

Figure 6. - Schlieren photograph of flow over isentropic forebody with diffuser cowl removed.

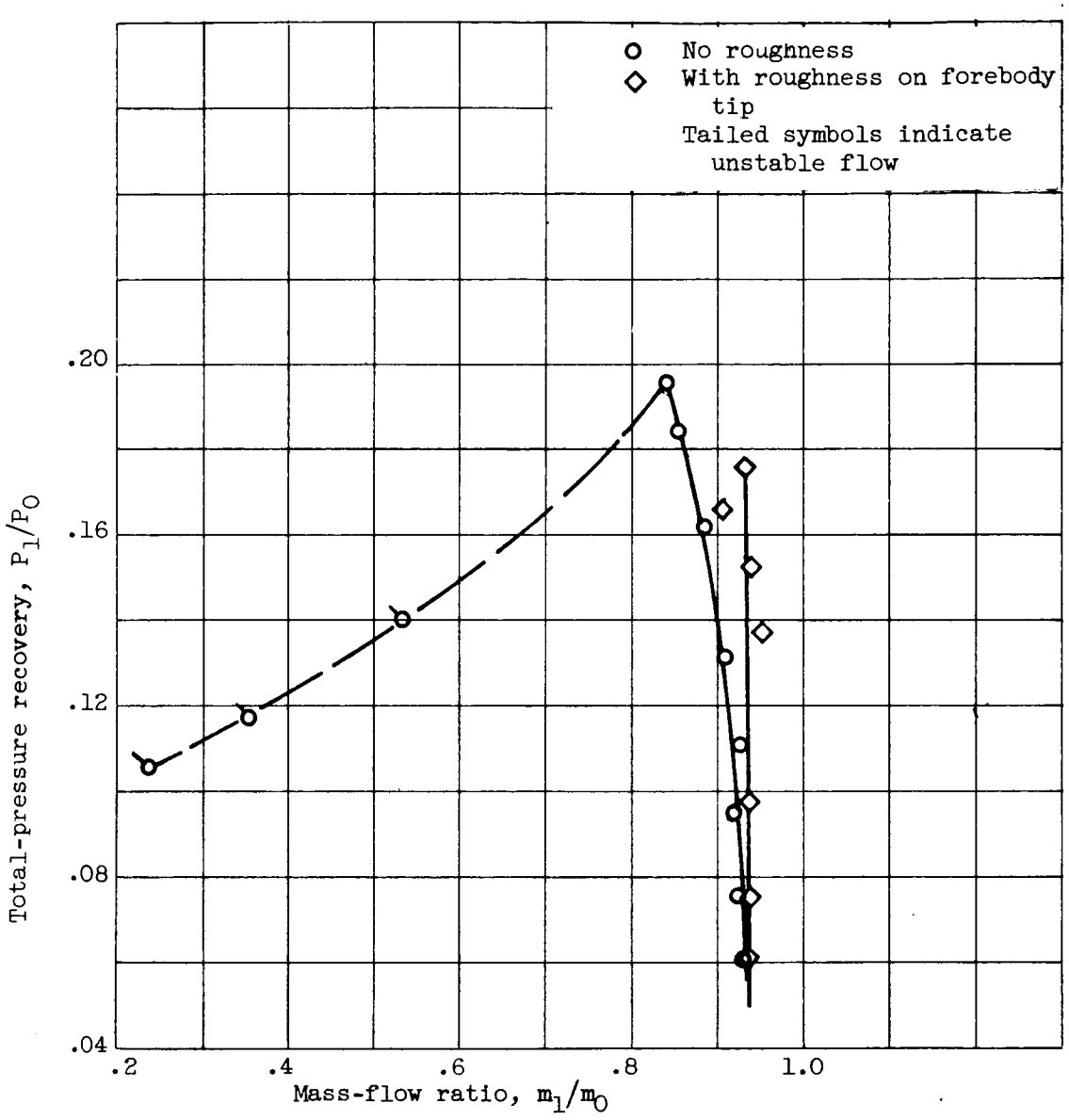

Figure 7. - Diffuser performance at zero angle of attack. Cowl A; forebody A; zero forebody translation.

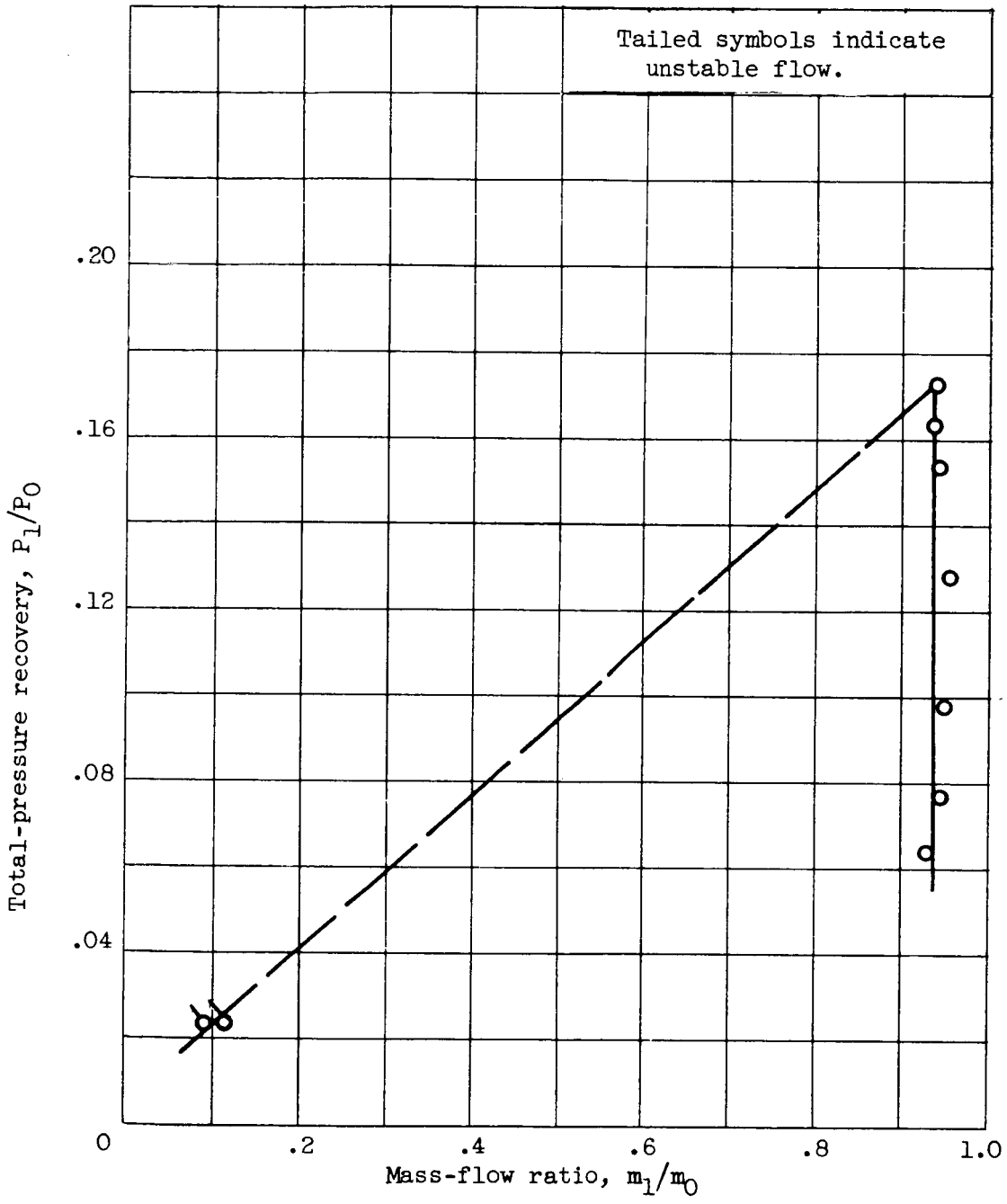

Figure 8. - Diffuser performance at 3° angle of attack. Cowl A; forebody A; zero forebody translation; no roughness.

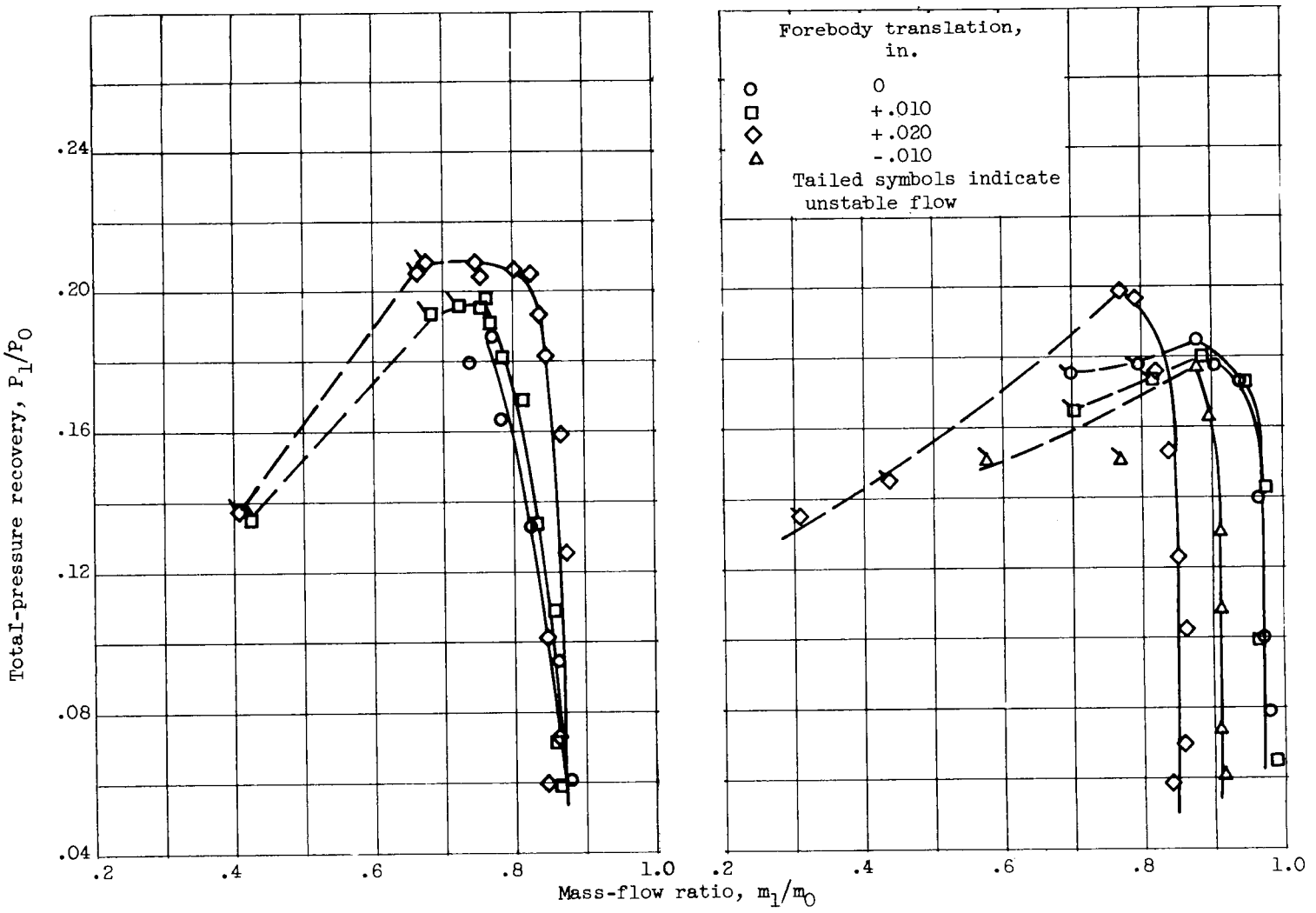

(a) No roughness.

(b) Roughness on forebody tip.

Figure 9. - Diffuser performance at zero angle of attack. Cowl B; forebody A.

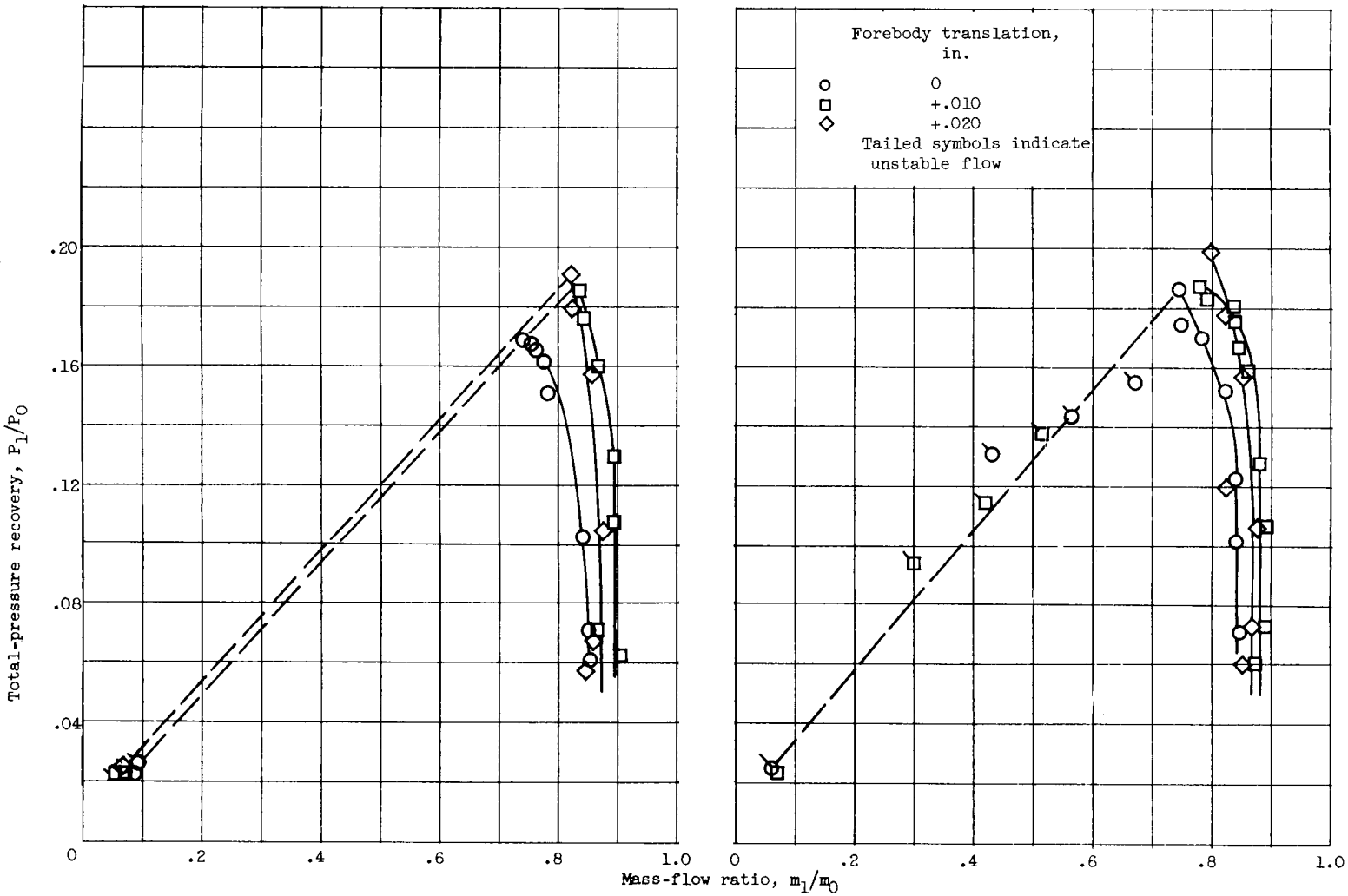

(a) No roughness.

(b) Roughness on forebody tip.

Figure 10. - Diffuser performance at 3° angle of attack. Cowl B; forebody A.

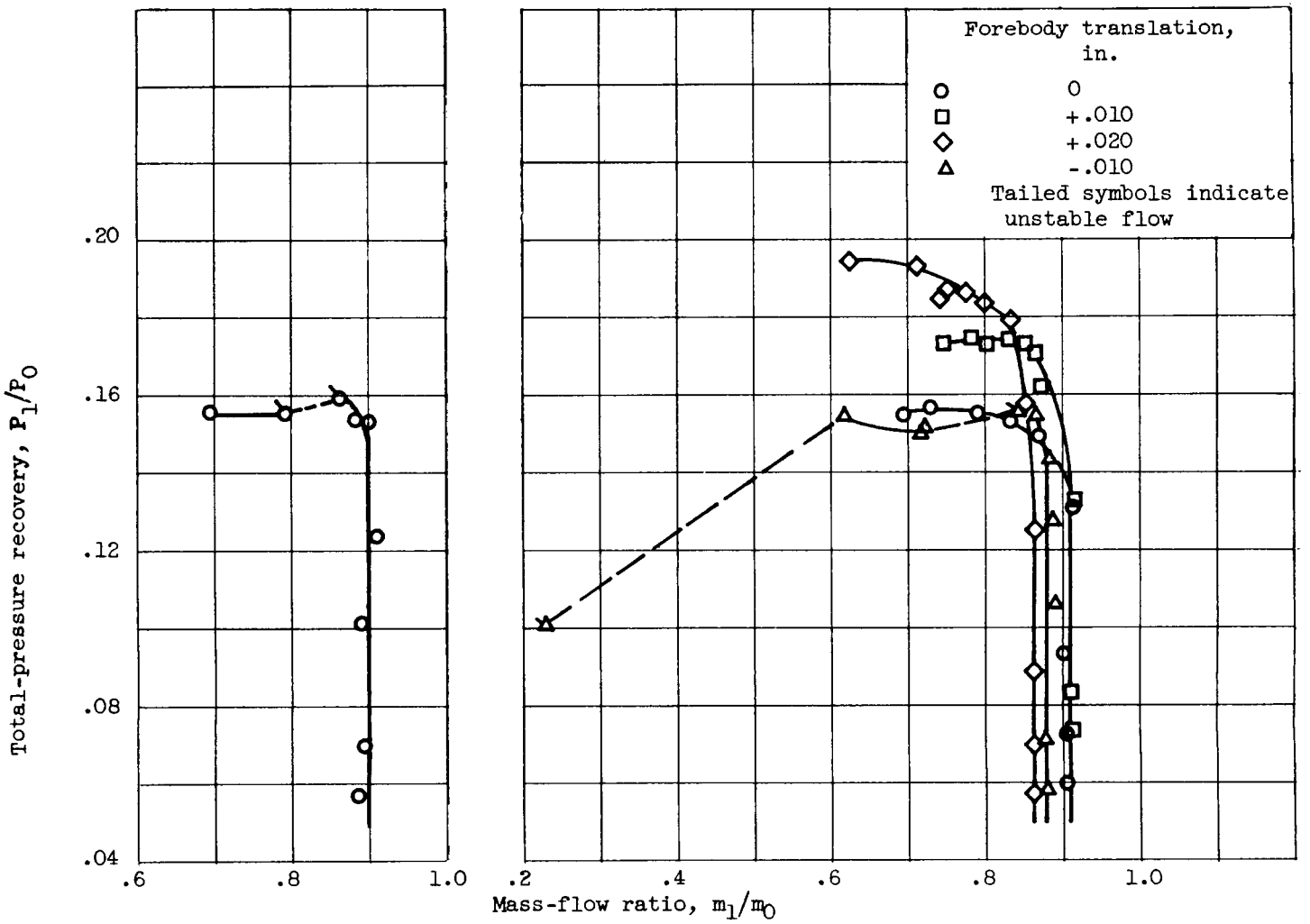

(a) No roughness.

(b) Roughness on forebody tip.

Figure 11. - Diffuser performance at zero angle of attack. Cowl B; forebody B.

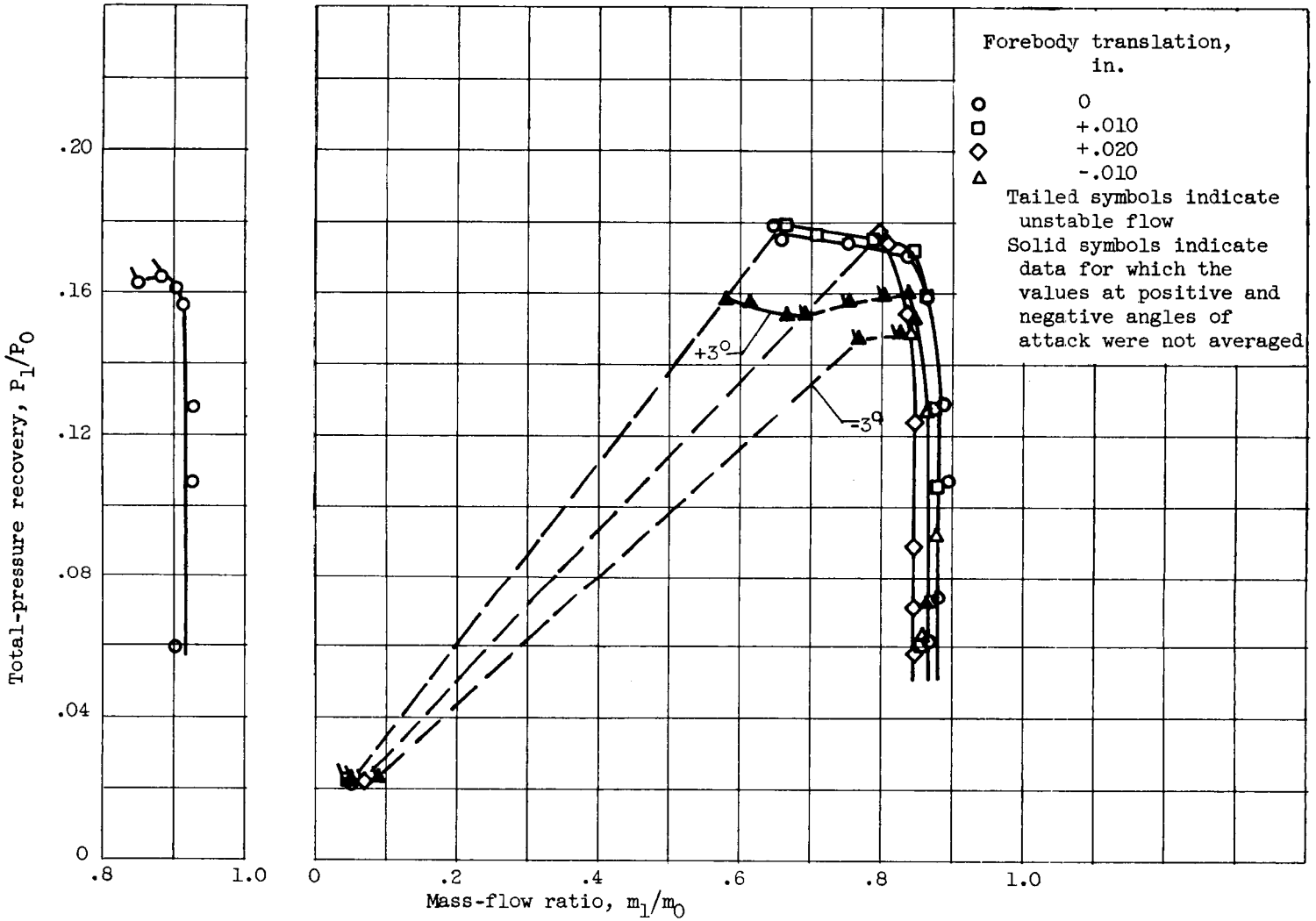

(a) No roughness.

(b) Roughness on forebody tip.

Figure 12. - Diffuser performance at 3° angle of attack. Cowl B; forebody B.

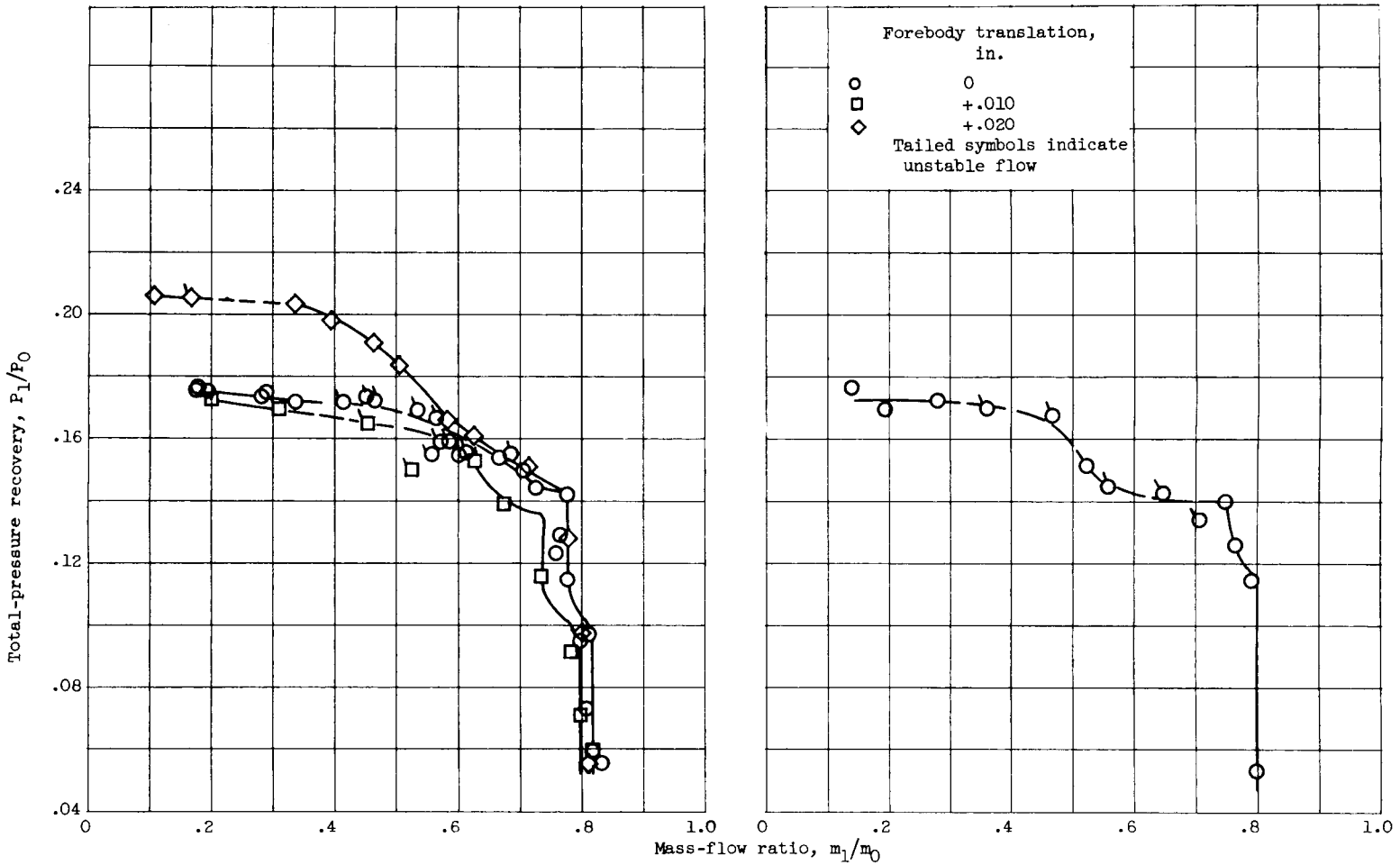

(a) Zero angle of attack.

(b) Angle of attack, 3°.

Figure 13. - Diffuser performance with bleed through forebody orifices. Cowl B; forebody B; roughness on forebody tip.

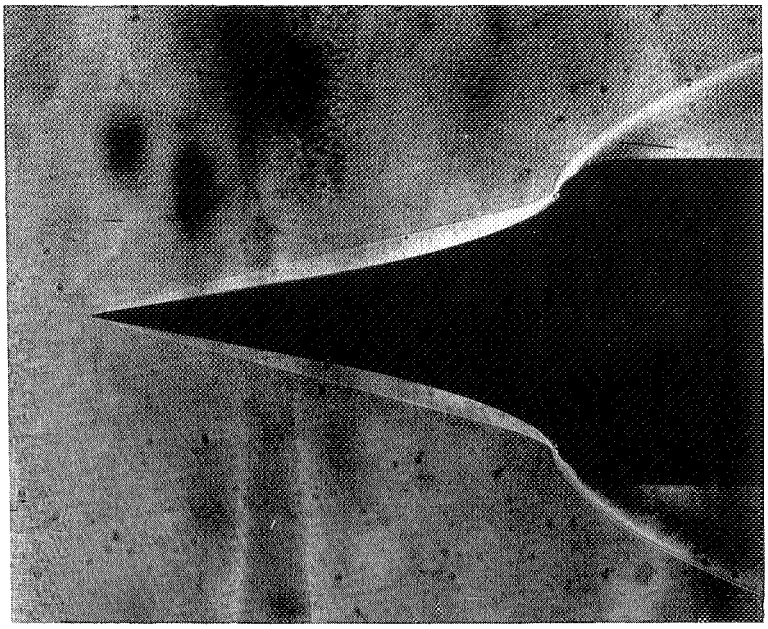

(a) No roughness.

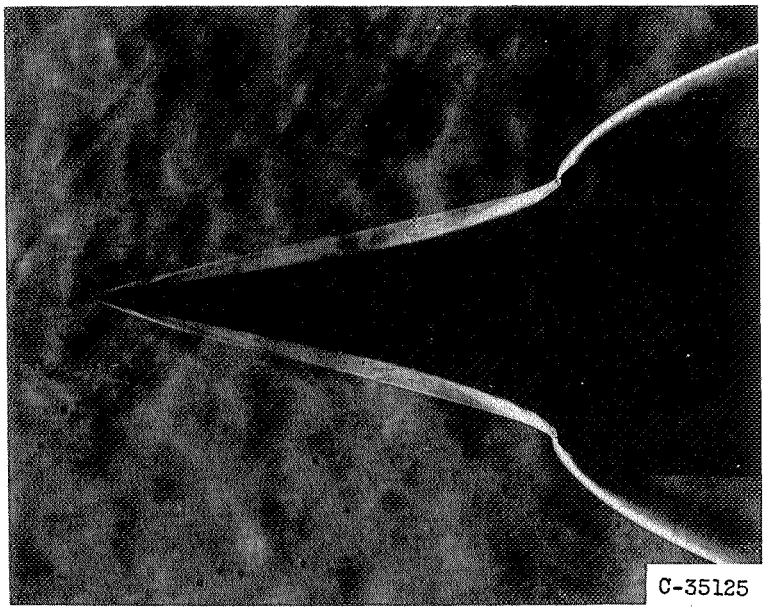

(b) Roughness on forebody tip.

Figure 14. - Schlieren photographs of diffuser at zero angle of attack. Stable flow.

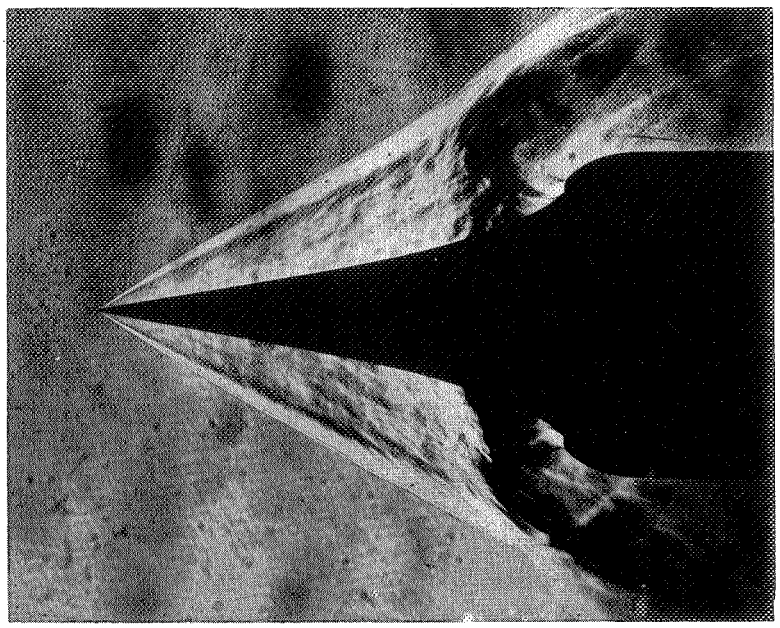

(a) No roughness.

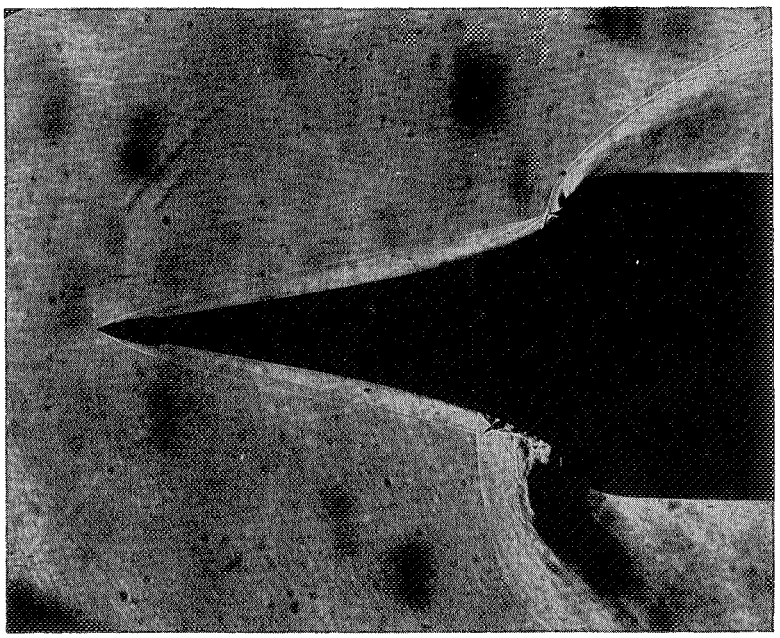

(b) Roughness. C-35126

Figure 15. - Elimination of flow separation during unstable flow by using roughness on forebody tip. Zero angle of attack.

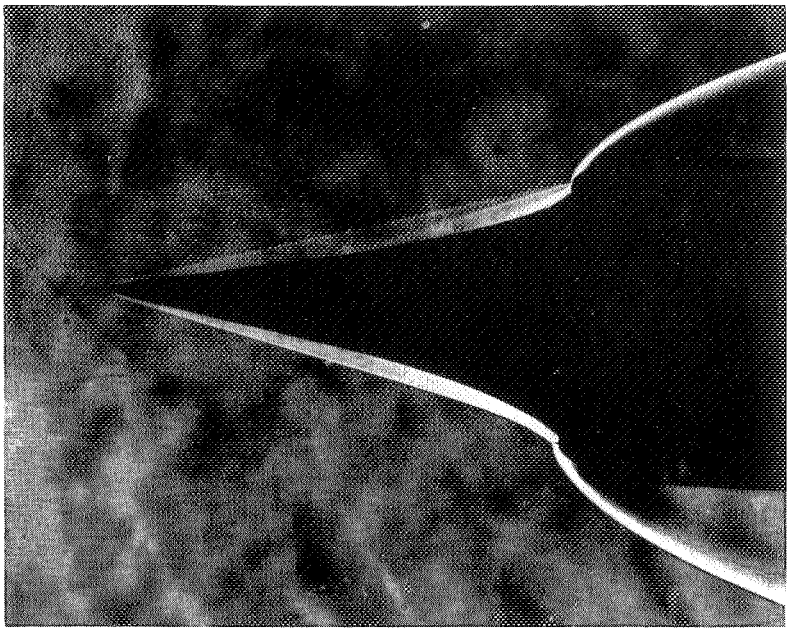

(a) No roughness.

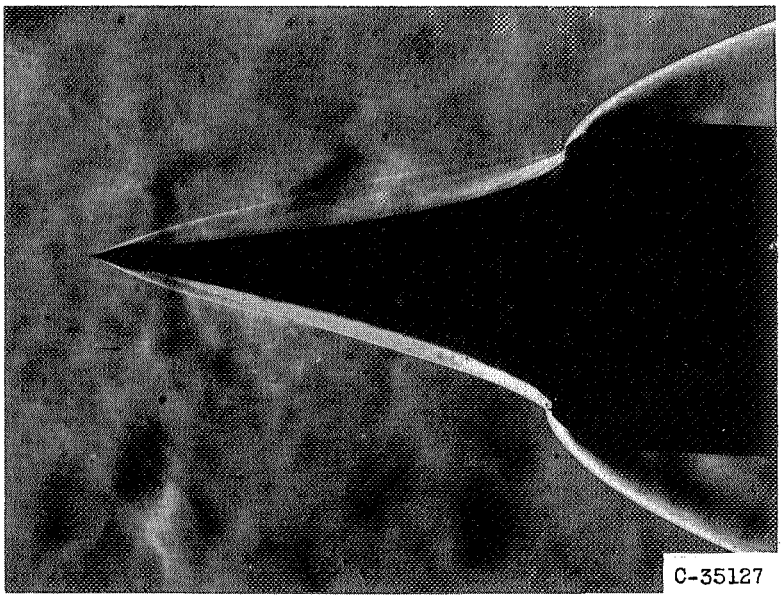

(b) Roughness.

Figure 16. - Schlieren photographs of diffuser at 3° angle of attack. Stable flow.

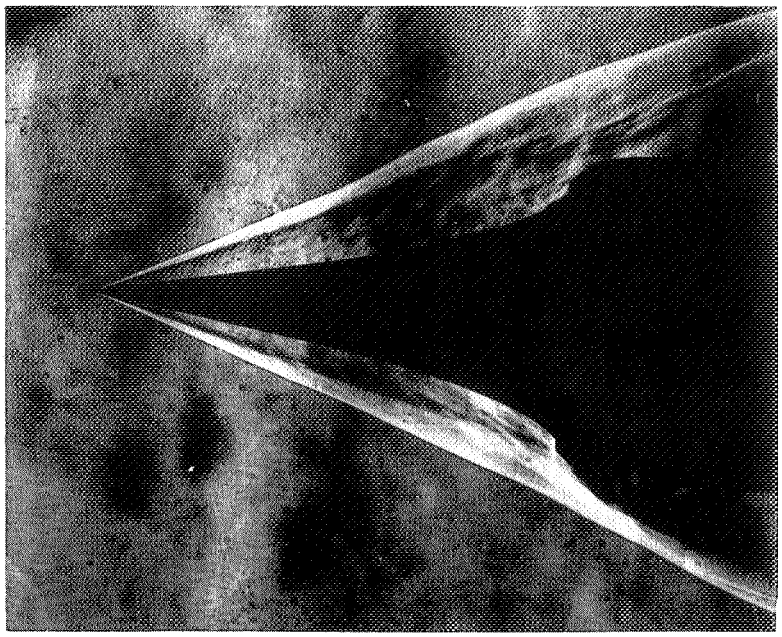

(a) No roughness.

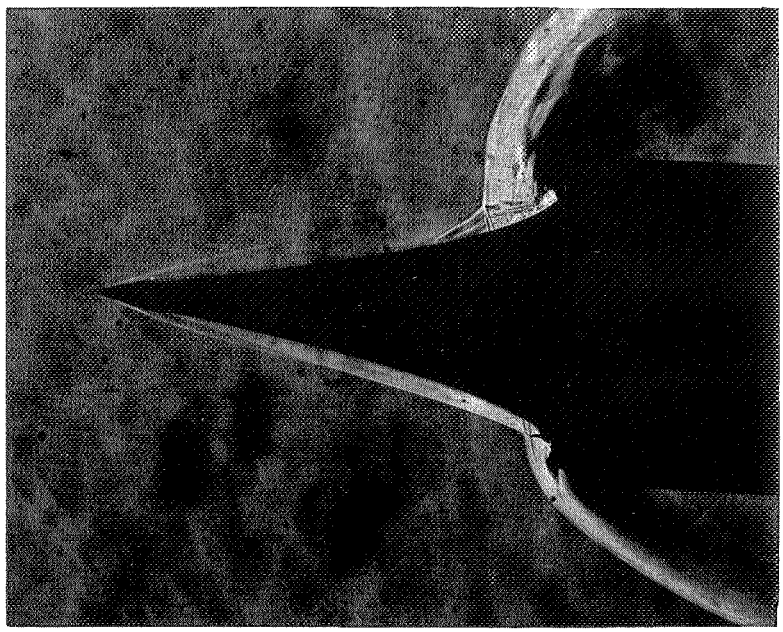

(b) Roughness.

C-35128

Figure 17. - Elimination of flow separation during unstable operation by using roughness on forebody tip. Angle of attack, 3°.

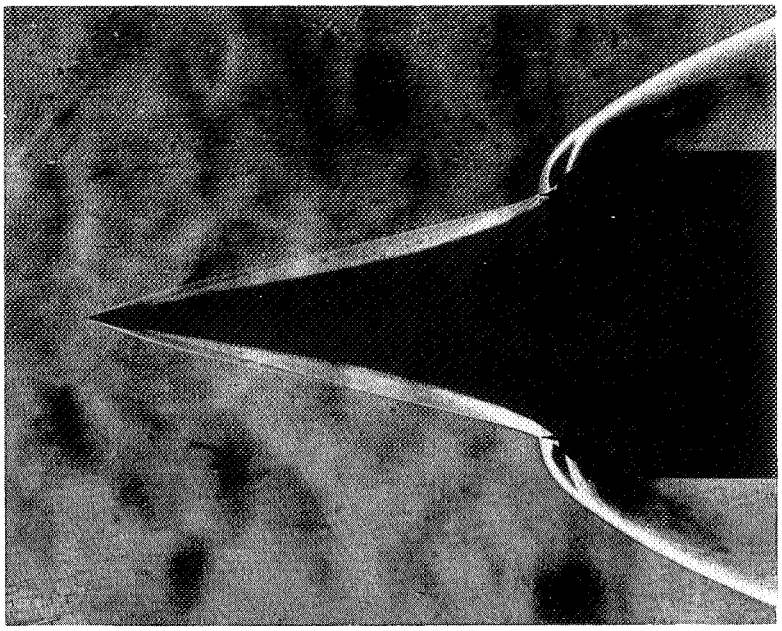

(a) Zero angle of attack.

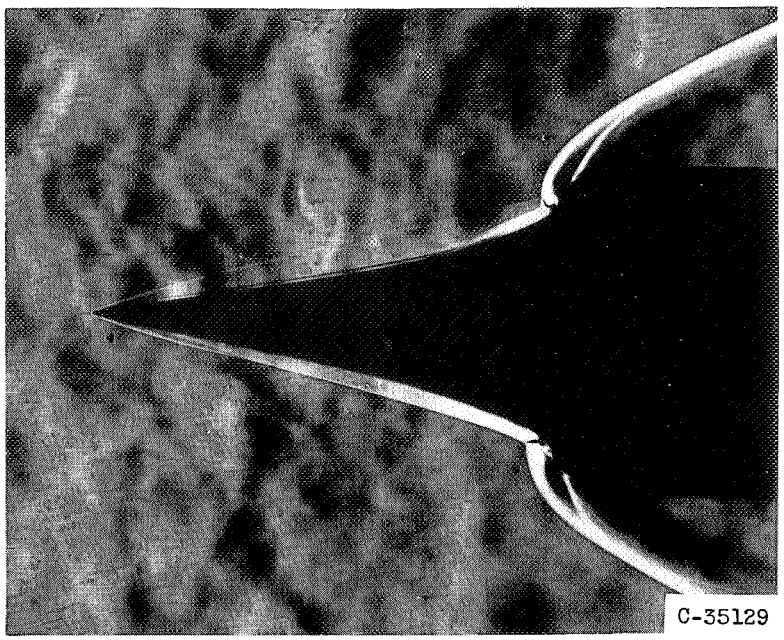

(b) Angle of attack, 3°.

Figure 18. - Schlieren photographs of diffuser with cowl B and forebody B showing operation at minimum stable mass flow. Forebody translation, -0.010 inch; roughness on forebody tip.

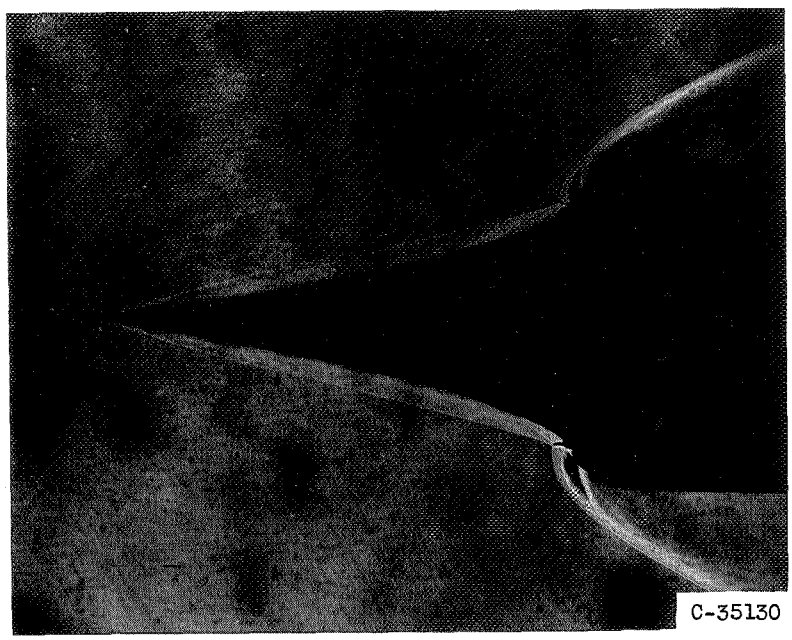

Figure 19. - Schlieren photograph of diffuser at 3° angle of attack with bleed through forebody orifices showing operation at minimum stable mass flow. Cowl B; forebody B; zero forebody translation; roughness on forebody tip.

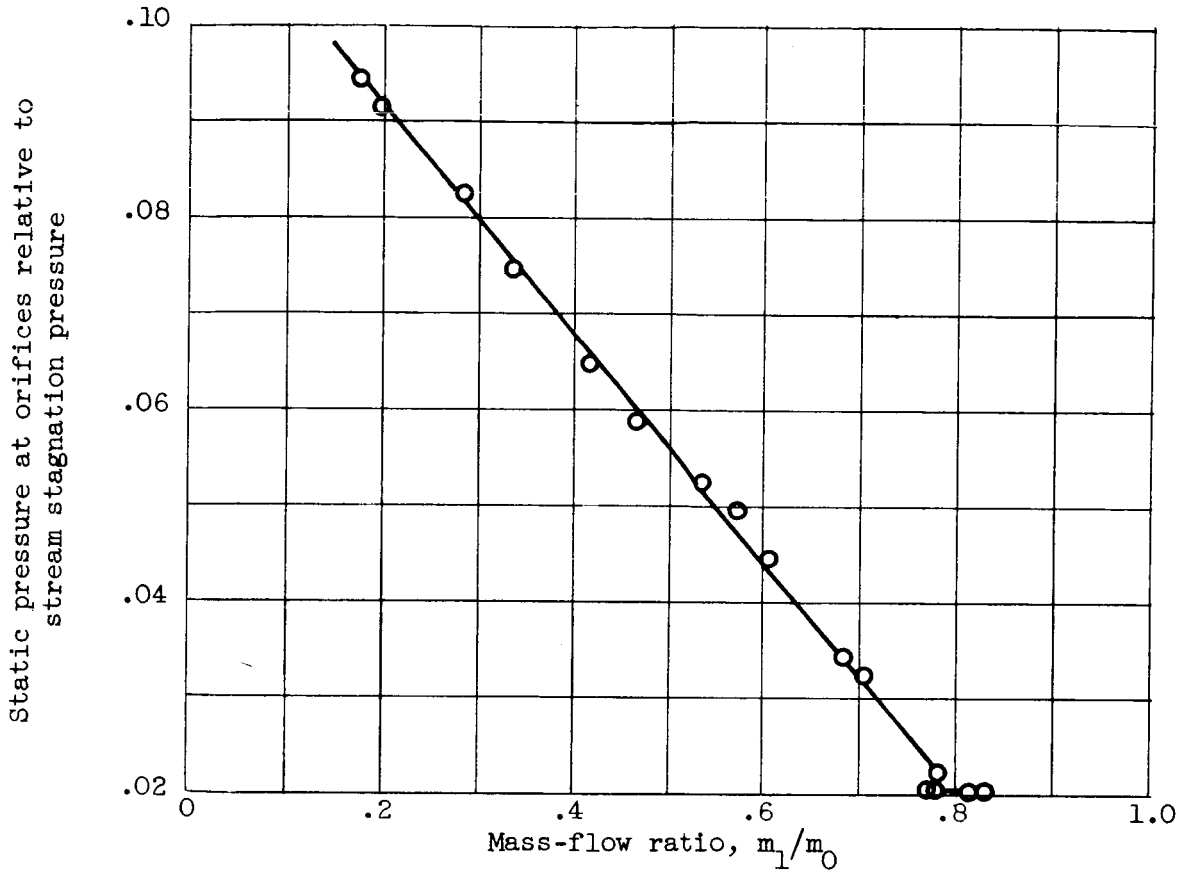

Figure 20. - Typical variation of measured static pressure at forebody orifices.